Photonics-Assisted Simultaneous RF Channelization and Self-Interference Cancellation

Xiaopeng Hu, Dan Zhu, *Member, IEEE*, Shuo Liu, Hai Xiao, and Shilong Pan, *Fellow, IEEE, Fellow, OSA*

***Abstract*—Both RF channelization and self-interference cancellation are urgently required for modern in-band full-duplex systems. A photonics-assisted RF receiver for simultaneous wideband channelization and self-interference cancellation is proposed and demonstrated. The key is the implementation of dual optical frequency combs (OFCs) followed by microwave photonic image-reject mixers (IRMs) using a dual-output Hartley structure. The received RF signal and the reference signal are modulated to a pair of signal OFCs with orthogonal polarization states, respectively. The microwave photonic IRM is applied on each polarization state, respectively. For each local OFC comb line, two components will be sliced and downconverted from each copy of the optically-carried received RF signal. Meanwhile, another two components will be sliced and downconverted from the optically-carried reference signal. After combining the outputs of the IRMs, the components from the image signal and the self-interference signal will be eliminated simultaneously. Two channels of the signal of interest will be obtained for each local OFC comb line. Experimental results show that an RF signal with an instantaneous bandwidth of 6 GHz (from 7 to 13 GHz) is channelized into 6 channels, each of which has a 1–GHz bandwidth. The isolation of larger than 28 dB between the channels is realized, and the simultaneous self-interference cancellation and image-rejection are achieved.**

***Index Terms*—Channelization, image-reject mixing, interference suppression, microwave photonics, optical frequency comb.**

I. Introduction

With the increasing requirements on spectrum resources in modern RF systems such as wireless communication, continuous-wave radar, electronic warfare, and cognitive systems, the in-band full-duplex (IBFD) technique has drawn a lot of attention due to its capability of improving the spectrum utilization efficiency [1], [2], [3], [4]. For an IBFD transceiver, two fundamental functions of RF channelization and self-interference cancellation are urgently needed when processing a wideband RF signal. On one hand, the wideband signal processing gives a great challenge with high sampling rates of the analog-to-digital converter (ADC). RF channelization offers a feasible solution to overcome this challenge, by which a broadband signal can be sliced into multiple narrowband channels [5]. It greatly alleviates the difficulty of wideband signal processing, and therefore reduces the hardware requirements with the ADCs. On the other hand, self-interference is regarded as one of the biggest impediments enabling IBFD operation. It is caused by the insufficient isolation between the transmitter and the receiver. Traditional filtering does not work since the self-interference and the signal of interest are on the same or overlapping frequencies. Consequently, self-interference cancellation is essential in an IBFD receiver.

Either photonics-based RF channelization techniques [6], [7], [8], [9], [10], [11], [12], [13] or self-interference cancellation techniques [14], [15], [16], [17], [18], [19], [20], [21], [22], [23], [24], [25] have been widely investigated in recent years, due to the advantages of broad working bandwidth and low transmission loss introduced by photonics. Microwave photonic channelization techniques can be mainly summarized into two categories. One method is to divide the optically-carried RF signal into multiple parts in the optical domain by using a set of optical filters [6], [7], [8], [9]. However, it gives strict demands with the optical filters on the aspects of flat-top responses and sharp roll-off characteristics, as well as the wavelength alignment of the periodical filters, which are hard to be satisfied. The other method is to convert the received RF signal and a local oscillator (LO) signal into the optical domain by using coherent dual optical frequency combs (OFCs) [10], [11], [12], [13]. After mixing the modulated OFCs, the different frequency components of the received RF signal are downconverted to the intermediate frequency (IF) band, and output from the corresponding channels.

To realize microwave photonic self-interference cancellation, an additional optical path containing a reference signal is introduced to subtract the self-interference signal in the analog optical domain [14]. Typically, the phase inversion between the self-interference signal and the reference signal can be realized by counter-biasing two electro-optic modulators [15], [16], [17], [18], [19], balanced detecting [20], [21], [22], or using microwave photonic phase shifters [23], [24], [25]. Recently, a microwave photonic channelized receiver with self-interference cancellation has been proposed in [26], for which the acousto-optic modulators are used to perform the frequency shifting of the optical LOs.

In this paper, a photonic approach for simultaneous RF channelization and self-interference cancellation is proposed and

Manuscript received 8 January 2023; revised 1 April 2023 and 24 April 2023; accepted 28 April 2023. Date of publication 5 May 2023; date of current version 19 September 2023. This work was supported in part by the National Natural Science Foundation of China under Grants 61971222 and 62271249, and in part by the Natural Science Foundation of Jiangsu Province under Grant BK20220076. *(Corresponding author: Dan Zhu.)*

This work did not involve human subjects or animals in its research.

The authors are with the College of Electronic and Information Engineering, Nanjing University of Aeronautics and Astronautics, Nanjing 210016, China (e-mail: hux@nuaa.edu.cn; danzhu@nuaa.edu.cn; liushuo_ls@nuaa.edu.cn; 664417873@nuaa.edu.cn; pans@nuaa.edu.cn).

Color versions of one or more figures in this article are available at https://doi.org/10.1109/JLT.2023.3273244.

Digital Object Identifier 10.1109/JLT.2023.3273244

demonstrated. The key is the implementation of dual OFCs followed by a dual-polarization 90-degree optical hybrid. The received RF signal and the reference signal are separately modulated to a pair of signal OFCs with orthogonal polarization states. A microwave photonic image-reject mixer (IRM) using a dual-output Hartley structure is applied on each separate polarization state, respectively. For each local OFC comb line, two components will be sliced and downconverted from the received RF signal modulated at the signal OFC with one polarization state. Meanwhile, another two components will be sliced and downconverted from the reference signal modulated at the signal OFC with the orthogonal polarization state correspondingly. After combining the outputs of the two IRMs for the received RF signal and the reference signal, the unwanted in-band interferences of the image signal and the self-interference are eliminated simultaneously. Two channels with the components of the required signal of interest will be obtained for each local OFC comb line. By introducing microwave photonic IRMs using a dual-output Hartley structure, the required optical spectrum resources are reduced by half. What's more, since the matching of the phase, time delay, and amplitude among the microwave photonic channelization paths, and between the reference signal and the self-interference signal are all implemented by photonic methods, wideband channelization and self-interference cancellation performances can be guaranteed. An experiment is carried out. A wideband linear frequency modulated (LFM) signal with a 6–GHz bandwidth is channelized to 6 channels. The isolation of larger than 28 dB between the channels is realized, and the simultaneous self-interference cancellation and image-rejection are achieved.

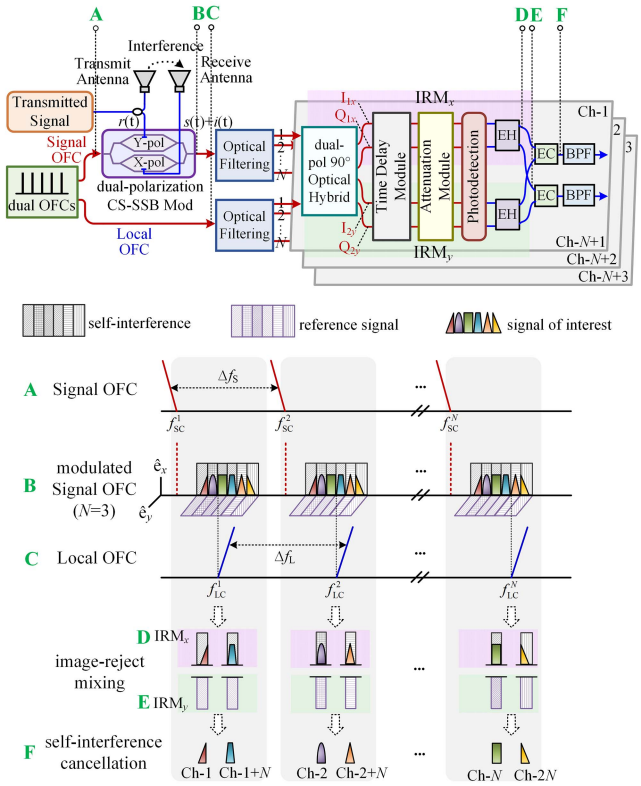

Fig. 1. Schematic diagram of the proposed photonics-assisted approach for simultaneous RF channelization and self-interference cancellation. OFC: optical frequency comb; CS-SSB mod: carrier-suppressed single-sideband modulation; IRM: image-reject mixer; EH: electrical hybrid; EC: electrical coupler; BPF: bandpass filter.

II. Principles

Fig. 1 illustrates the proposed photonics-assisted in-band full-duplex RF receiver which can realize simultaneous RF channelization and self-interference cancellation. Two OFCs with N comb lines are used as the signal OFC and the local OFC, respectively. The frequency intervals between the adjacent comb lines are Δf_{S} and Δf_{L} with the signal OFC and the local OFC, respectively, where $\Delta f_{\mathrm{L}} = \Delta f_{\mathrm{S}} + \Delta f$. The frequency values of the n^{th} comb lines of the signal OFC (f_n SC) and the local OFC (f_n LC) are given by

$$\begin{cases} f_{\mathrm{SC}}^{n} = f_{\mathrm{SC}}^{1} + (n-1)\Delta f_{\mathrm{s}} \\ f_{\mathrm{LC}}^{n} = f_{\mathrm{LC}}^{1} + (n-1)\Delta f_{\mathrm{L}} \\ \quad\;\; = f_{\mathrm{SC}}^{1} + \Delta f_1 + (n-1)(\Delta f_{\mathrm{s}} + \Delta f) \end{cases} \tag{1}$$

where f_{SC}^{1} and f_{LC}^{1} are the frequencies of the 1st comb lines of the signal OFC and local OFC, respectively, and Δf_1 is the frequency difference between f_{SC}^{1} and f_{LC}^{1}.

The signal OFC is then sent to a dual-polarization carrier-suppressed single-sideband (CS-SSB) modulator, at which the received RF signal and the reference signal are modulated onto one side of each comb line of the signal OFCs with orthogonal polarization states. The received RF signal consists of the signal of interest and the self-interference signal. The optically-carried signal at the n^{th} comb line of the modulated signal OFC can be written as

$$\begin{aligned} f_{\mathrm{S\,mod}}^{n} &= \hat{\mathrm{e}}_x \cdot \{[f_{\mathrm{SC}}^{n} + f_{\mathrm{SOI}}(t)] + [f_{\mathrm{SC}}^{n} + f_{\mathrm{SI}}(t-\tau_{\mathrm{SI}})]\} \\ &\quad + \hat{\mathrm{e}}_y \cdot [f_{\mathrm{SC}}^{n} + f_{\mathrm{Ref}}(t-\tau_{\mathrm{Ref}})] \\ &= \hat{\mathrm{e}}_x \cdot \{[f_{\mathrm{SC}}^{n} + f_{\mathrm{SOI,L}}^{n}(t)] + [f_{\mathrm{SC}}^{n} + f_{\mathrm{SOI,R}}^{n}(t)] \\ &\quad + [f_{\mathrm{SC}}^{n} + f_{\mathrm{SI,L}}^{n}(t-\tau_{\mathrm{SI}})] + [f_{\mathrm{SC}}^{n} + f_{\mathrm{SI,R}}^{n}(t-\tau_{\mathrm{SI}})]\} \\ &\quad + \hat{\mathrm{e}}_y \cdot \{[f_{\mathrm{SC}}^{n} + f_{\mathrm{Ref,L}}^{n}(t-\tau_{\mathrm{Ref}})] \\ &\quad + [f_{\mathrm{SC}}^{n} + f_{\mathrm{Ref,R}}^{n}(t-\tau_{\mathrm{Ref}})]\} \end{aligned} \tag{2}$$

where $\hat{\mathrm{e}}_x$ and $\hat{\mathrm{e}}_y$ represent the two orthogonally polarization states. $f_{\mathrm{SOI,L}}^{n}(t)$ and $f_{\mathrm{SOI,R}}^{n}(t)$ represent the frequency components of the optically-carried signal of interest located at the left and right sides of the local OFC's n^{th} comb line f_{LC}^{n}, respectively. $f_{\mathrm{SI,L}}^{n}(t)$ and $f_{\mathrm{SI,R}}^{n}(t)$ represent the frequency components of the optically-carried self-interference signal located at the left and right sides of f_{LC}^{n}, respectively. $f_{\mathrm{Ref,L}}^{n}(t)$ and $f_{\mathrm{Ref,R}}^{n}(t)$ represent the frequency components of the optically-carried reference signal located at the left and right sides of f_{LC}^{n}, respectively. τ_{SI} and τ_{Ref} represent the time delays of the self-interference signal and the reference signal, respectively. Two multi-channel optical filters are utilized to separate the modulated signal OFC and the local OFC. The optical fields of the n^{th} outputs of the two optical filters can be expressed as (3) shown at the bottom of the next page, where a_n, b_n, and c_n are the amplitudes of the corresponding optical sidebands. Then, the separated optically-carried RF copies and the photonic LOs are fed into microwave photonic IRMs (IRM$_x$ and IRM$_y$) using a dual-output Hartley structure.

Each microwave photonic IRM consists of a 90-degree optical hybrid, two photodetectors (PDs), and a dual-output electrical hybrid. IRM$_x$ and IRM$_y$ share one single dual-polarization 90-degree optical hybrid through polarization multiplexing. At the input ports of the optical hybrid, the optically-carried RF copies will be polarization demultiplexed, while the photonic LOs will be power divided [27]. With the help of the 90-degree optical hybrid, two in-phase optical outputs ($I_{1x,y} \propto \hat{\mathrm{e}}_{x,y} E^n_{\mathrm{Sig}x,y} + E^n_{\mathrm{LO}}$, and $I_{2x,y} \propto \hat{\mathrm{e}}_{x,y} E^n_{\mathrm{Sig}x,y} - E^n_{\mathrm{LO}}$) and two quadrature optical outputs ($Q_{1x,y} \propto \hat{\mathrm{e}}_{x,y} E^n{}_{\mathrm{Sig}x,y} + \mathrm{j}E^n{}_{\mathrm{LO}}$, and $Q_{2x,y} \propto \hat{\mathrm{e}}_{x,y} E^n{}_{\mathrm{Sig}x,y} - \mathrm{j}E^n{}_{\mathrm{LO}}$) are achieved. A π-phase difference with the photonic LO is introduced for both the two in-phase (I_{1x} and I_{2y}) and the two quadrature (Q_{1x} and Q_{2y}) optical outputs. The four optical signals can be expressed as

$$\begin{cases} I_{1x}(t) \propto \hat{\mathrm{e}}_x \cdot E^n_{\mathrm{Sig}}(t) + E^n_{\mathrm{LO}}(t) \\ \propto \underbrace{\hat{\mathrm{e}}_x \cdot \left\{ a_n \mathrm{e}^{\mathrm{j}2\pi t\left[f^n_{\mathrm{SC}} + f^n_{\mathrm{SOI,L}}(t)\right]} + b_n \mathrm{e}^{\mathrm{j}2\pi t\left[f^n_{\mathrm{SC}} + f^n_{\mathrm{SI,L}}(t-\tau_{\mathrm{SI}})\right]} \right\}}_{\mathrm{the\,components\,with\,frequency} < f^n_{\mathrm{LC}}} \\ + \underbrace{\hat{\mathrm{e}}_x \cdot \left\{ a_n \mathrm{e}^{\mathrm{j}2\pi t\left[f^n_{\mathrm{SC}} + f^n_{\mathrm{SOI,R}}(t)\right]} + b_n \mathrm{e}^{\mathrm{j}2\pi t\left[f^n_{\mathrm{SC}} + f^n_{\mathrm{SI,R}}(t-\tau_{\mathrm{SI}})\right]} \right\}}_{\mathrm{the\,components\,with\,frequency} > f^n_{\mathrm{LC}}} \\ + \mathrm{e}^{\mathrm{j}2\pi f^n_{\mathrm{LC}} t} \\ Q_{1x}(t) \propto \hat{\mathrm{e}}_x \cdot E^n_{\mathrm{Sig}}(t) + \mathrm{j}E^n_{\mathrm{LO}}(t) \\ \propto \underbrace{\hat{\mathrm{e}}_x \cdot \left\{ a_n \mathrm{e}^{\mathrm{j}2\pi t\left[f^n_{\mathrm{SC}} + f^n_{\mathrm{SOI,L}}(t)\right]} + b_n \mathrm{e}^{\mathrm{j}2\pi t\left[f^n_{\mathrm{SC}} + f^n_{\mathrm{SI,L}}(t-\tau_{\mathrm{SI}})\right]} \right\}}_{\mathrm{the\,components\,with\,frequency} < f^n_{\mathrm{LC}}} \\ + \underbrace{\hat{\mathrm{e}}_x \cdot \left\{ a_n \mathrm{e}^{\mathrm{j}2\pi t\left[f^n_{\mathrm{SC}} + f^n_{\mathrm{SOI,R}}(t)\right]} + b_n \mathrm{e}^{\mathrm{j}2\pi t\left[f^n_{\mathrm{SC}} + f^n_{\mathrm{SI,R}}(t-\tau_{\mathrm{SI}})\right]} \right\}}_{\mathrm{the\,components\,with\,frequency} > f^n_{\mathrm{LC}}} \\ + \mathrm{j}\mathrm{e}^{\mathrm{j}2\pi f^n_{\mathrm{LC}} t} \\ I_{2y}(t) \propto \hat{\mathrm{e}}_y \cdot E^n_{\mathrm{Sig}}(t) - E^n_{\mathrm{LO}}(t) \\ \propto \underbrace{\hat{\mathrm{e}}_y \cdot c_n \mathrm{e}^{\mathrm{j}2\pi t\left[f^n_{\mathrm{SC}} + f^n_{\mathrm{Ref,L}}(t-\tau_{\mathrm{Ref}})\right]}}_{\mathrm{the\,components\,with\,frequency} < f^n_{\mathrm{LC}}} \\ + \underbrace{\hat{\mathrm{e}}_y \cdot c_n \mathrm{e}^{\mathrm{j}2\pi t\left[f^n_{\mathrm{SC}} + f^n_{\mathrm{Ref,R}}(t-\tau_{\mathrm{Ref}})\right]}}_{\mathrm{the\,components\,with\,frequency} > f^n_{\mathrm{LC}}} - \mathrm{e}^{\mathrm{j}2\pi f^n_{\mathrm{LC}} t} \\ Q_{2y}(t) \propto \hat{\mathrm{e}}_y \cdot E^n_{\mathrm{Sig}}(t) - \mathrm{j}E^n_{\mathrm{LO}}(t) \\ \propto \underbrace{\hat{\mathrm{e}}_y \cdot c_n \mathrm{e}^{\mathrm{j}2\pi t\left[f^n_{\mathrm{SC}} + f^n_{\mathrm{Ref,L}}(t-\tau_{\mathrm{Ref}})\right]}}_{\mathrm{the\,components\,with\,frequency} < f^n_{\mathrm{LC}}} \\ + \underbrace{\hat{\mathrm{e}}_y \cdot c_n \mathrm{e}^{\mathrm{j}2\pi t\left[f^n_{\mathrm{SC}} + f^n_{\mathrm{Ref,R}}(t-\tau_{\mathrm{Ref}})\right]}}_{\mathrm{the\,components\,with\,frequency} > f^n_{\mathrm{LC}}} - \mathrm{j}\mathrm{e}^{\mathrm{j}2\pi f^n_{\mathrm{LC}} t} \end{cases} \tag{4}$$

The optical outputs of I_{1x}, Q_{1x}, I_{2y}, and Q_{2y} are then sent to an optical time delay module and an optical attenuation module to realize the time delay and amplitude matchings between the four paths. After performing photodetection with these optical signals, two pairs of downconverted quadrature electrical outputs are obtained as follows

$$\begin{cases} i_{\mathrm{I}_{1x}} \propto \Re_1 \eta_1 \left\{ a_n \cos 2\pi \left[f^n_{\mathrm{LO}} - f^n_{\mathrm{SOI,L}}(t-\tau_1) \right] \right. \\ \quad + b_n \cos 2\pi \left[f^n_{\mathrm{LO}} - f^n_{\mathrm{SI,L}}(t-\tau_{\mathrm{SI}}-\tau_1) \right] \\ \quad + a_n \cos 2\pi \left[f^n_{\mathrm{SOI,R}}(t-\tau_1) - f^n_{\mathrm{LO}} \right] \\ \quad \left. + b_n \cos 2\pi \left[f^n_{\mathrm{SI,R}}(t-\tau_{\mathrm{SI}}-\tau_1) - f^n_{\mathrm{LO}} \right] \right\} \\ i_{\mathrm{Q}_{1x}} \propto \Re_2 \eta_2 \left\{ -a_n \sin 2\pi \left[f^n_{\mathrm{LO}} - f^n_{\mathrm{SOI,L}}(t-\tau_2) \right] \right. \\ \quad - b_n \sin 2\pi \left[f^n_{\mathrm{LO}} - f^n_{\mathrm{SI,L}}(t-\tau_{\mathrm{SI}}-\tau_2) \right] \\ \quad + a_n \sin 2\pi \left[f^n_{\mathrm{SOI,R}}(t-\tau_2) - f^n_{\mathrm{LO}} \right] \\ \quad \left. + b_n \sin 2\pi \left[f^n_{\mathrm{SI,R}}(t-\tau_{\mathrm{SI}}-\tau_2) - f^n_{\mathrm{LO}} \right] \right\} \\ i_{\mathrm{I}_{2y}} \propto \Re_3 \eta_3 \left\{ -c_n \cos 2\pi \left[f^n_{\mathrm{LO}} - f^n_{\mathrm{Ref,L}}(t-\tau_{\mathrm{Ref}}-\tau_3) \right] \right. \\ \quad \left. - c_n \cos 2\pi \left[f^n_{\mathrm{Ref,R}}(t-\tau_{\mathrm{Ref}}-\tau_3) - f^n_{\mathrm{LO}} \right] \right\} \\ i_{\mathrm{Q}_{2y}} \propto \Re_4 \eta_4 \left\{ c_n \sin 2\pi \left[f^n_{\mathrm{LO}} - f^n_{\mathrm{Ref,L}}(t-\tau_{\mathrm{Ref}}-\tau_4) \right] \right. \\ \quad \left. - c_n \sin 2\pi \left[f^n_{\mathrm{Ref,R}}(t-\tau_{\mathrm{Ref}}-\tau_4) - f^n_{\mathrm{LO}} \right] \right\} \end{cases} \tag{5}$$

where $f^n_{\mathrm{LO}} = f^n_{\mathrm{LC}} - f^n_{\mathrm{SC}} = \Delta f_1 + (n-1)\Delta f$. $\Re_{1,2,3,4}$ represent the responsivity of corresponding photodetectors. $\tau_{1,2,3,4}$ and $\eta_{1,2,3,4}$ represent the power attenuation coefficient of the optical attenuation module and the time delay of the four optical outputs, respectively. By properly tuning the optical time delay module to make $\tau_1 = \tau_2$ and $\tau_3 = \tau_4$, the π-phase difference with the photonic LO for the two in-phase (I_{1x} and I_{2y}) and the two quadrature (Q_{1x} and Q_{2y}) optical outputs is mapped to the IF signals. In this way, the phase inversion is realized. By properly tuning the optical attenuation module to make $\Re_1\eta_1 = \Re_2\eta_2$ and $\Re_3\eta_3 = \Re_4\eta_4$, and using two dual-output electrical hybrids to combine the two pairs of quadrature outputs, respectively, the two outputs of IRM$_x$ are given by

$$\begin{cases} i_{11} = i_{\mathrm{I}_{1x}} \angle \frac{\pi}{2} + i_{\mathrm{Q}_{1x}} \angle 0 \\ \quad = -2\Re_1\eta_1 a_n \sin 2\pi \left[f^n_{\mathrm{LO}} - f^n_{\mathrm{SOI,L}}(t-\tau_1) \right] \\ \quad -2\Re_1\eta_1 b_n \sin 2\pi \left[f^n_{\mathrm{LO}} - f^n_{\mathrm{SI,L}}(t-\tau_{\mathrm{SI}}-\tau_1) \right] \\ i_{12} = i_{\mathrm{I}_{1x}} \angle 0 + i_{\mathrm{Q}_{1x}} \angle \frac{\pi}{2} \\ \quad = 2\Re_1\eta_1 a_n \cos 2\pi \left[f^n_{\mathrm{SOI,R}}(t-\tau_1) - f^n_{\mathrm{LO}} \right] \\ \quad +2\Re_1\eta_1 b_n \cos 2\pi \left[f^n_{\mathrm{SI,R}}(t-\tau_{\mathrm{SI}}-\tau_1) - f^n_{\mathrm{LO}} \right] \end{cases} \tag{6}$$

Meanwhile, the two outputs of IRM$_y$ are given by

$$\begin{cases} i_{21} = i_{\mathrm{I}_{2y}} \angle \frac{\pi}{2} + i_{\mathrm{Q}_{2y}} \angle 0 \\ \quad = 2\Re_3\eta_3 c_n \sin 2\pi \left[f^n_{\mathrm{LO}} - f^n_{\mathrm{Ref,L}}(t-\tau_{\mathrm{Ref}}-\tau_3) \right] \\ i_{22} = i_{\mathrm{I}_{2y}} \angle 0 + i_{\mathrm{Q}_{2y}} \angle \frac{\pi}{2} \\ \quad = -2\Re_3\eta_3 c_n \cos 2\pi \left[f^n_{\mathrm{Ref,R}}(t-\tau_{\mathrm{Ref}}-\tau_3) - f^n_{\mathrm{LO}} \right] \end{cases} \tag{7}$$

$$\begin{cases} E^n_{\mathrm{Sig}}(t) \propto \mathrm{e}^{\mathrm{j}2\pi f^n_{\mathrm{S\,mod}} t} \\ = \underbrace{\hat{\mathrm{e}}_x \cdot \left\{ a_n \mathrm{e}^{\mathrm{j}2\pi t\left[f^n_{\mathrm{SC}} + f^n_{\mathrm{SOI,L}}(t)\right]} + b_n \mathrm{e}^{\mathrm{j}2\pi t\left[f^n_{\mathrm{SC}} + f^n_{\mathrm{SI,L}}(t-\tau_{\mathrm{SI}})\right]} \right\} + \hat{\mathrm{e}}_y \cdot c_n \mathrm{e}^{\mathrm{j}2\pi t\left[f^n_{\mathrm{SC}} + f^n_{\mathrm{Ref,L}}(t-\tau_{\mathrm{Ref}})\right]}}_{\mathrm{the\,components\,with\,frequency} < f^n_{\mathrm{LC}}} \\ + \underbrace{\hat{\mathrm{e}}_x \cdot \left\{ a_n \mathrm{e}^{\mathrm{j}2\pi t\left[f^n_{\mathrm{SC}} + f^n_{\mathrm{SOI,R}}(t)\right]} + b_n \mathrm{e}^{\mathrm{j}2\pi t\left[f^n_{\mathrm{SC}} + f^n_{\mathrm{SI,R}}(t-\tau_{\mathrm{SI}})\right]} \right\} + \hat{\mathrm{e}}_y \cdot c_n \mathrm{e}^{\mathrm{j}2\pi t\left[f^n_{\mathrm{SC}} + f^n_{\mathrm{Ref,R}}(t-\tau_{\mathrm{Ref}})\right]}}_{\mathrm{the\,components\,with\,frequency} > f^n_{\mathrm{LC}}} \\ E^n_{\mathrm{LO}}(t) \propto \mathrm{e}^{\mathrm{j}2\pi f^n_{\mathrm{LC}} t} \end{cases} \tag{3}$$

As can be seen from (6) and (7), IRM$_x$ outputs the downconverted received RF signal (i_{11} and i_{12}), while IRM$_y$ outputs the downconverted reference signal (i_{21} and i_{22}). The downconverted frequency components from the left and right sides of the photonic LO ($f^n_{\mathrm{SOI,L}}/f^n_{\mathrm{SOI,R}}$, $f^n_{\mathrm{SI,L}}/f^n_{\mathrm{SI,R}}$, and $f^n_{\mathrm{Ref,L}}/f^n_{\mathrm{Ref,R}}$) would be output from different output ports of each IRM, and the image-reject mixing is achieved. Then, one electrical coupler is used to combine i_{11} and i_{21}, while the other one is used to combine i_{12} and i_{22}. Since $f^n_{\mathrm{Ref}} = f^n_{\mathrm{SI}}$, when $\Re_1\eta_1 a_n = \Re_3\eta_3 c_n$ and τ_3-$\tau_1 = \tau_{\mathrm{Ref}}$-$\tau_{\mathrm{SI}}$, the outputs of the two couplers can be written as

$$\begin{cases} i_{\mathrm{EC1}} = i_{11} + i_{21} = -2\Re_1\eta_1 a_n \sin 2\pi \\ \left[f^n_{\mathrm{LO}} - f^n_{\mathrm{SOI,L}}(t-\tau_1)\right] \\ i_{\mathrm{EC2}} = i_{12} + i_{22} = 2\Re_1\eta_1 a_n \cos 2\pi \\ \left[f^n_{\mathrm{SOI,R}}(t-\tau_1) - f^n_{\mathrm{LO}}\right] \end{cases} \tag{8}$$

It can be seen from (8) that the self-interference signal has been removed, and only the required signal of interest remains. Thus, the self-interference cancellation is realized. Meanwhile, for different channels, each comb line of the local OFC aligns to different frequency components of the modulated signal OFC, thus the received signal of interest would be downconverted to the same IF band. An electrical bandpass filter (EBPF) is incorporated after each electrical coupler to filter out the out-of-band signals. Finally, two channelized frequency components corresponding to Ch-*n* and Ch-(*n*+*N*) are achieved. For the local/signal OFCs with *N* comb lines, the channelization with 2*N* independent output channels will be realized. Both the image interference and the self-interference are suppressed simultaneously in each channel. The image-reject mixing also guarantees the isolation between the two channels corresponding to the same photonic LO. In addition, as can be seen from (2)–(8), the system performances are independent of the signals' type. It is worthy to be noted that the proposed channelized receiver has great reconfigurable ability. The bandwidth of the channels can be easily changed by tuning the frequency intervals of the signal OFC (f_{S}) and local OFC (f_{L}). The number of the channels can be extended by increasing the number of the comb lines of the dual OFCs.

III. Experimental Results and Discussion

A. Experimental Setup

An experiment is carried out based on the setup shown in Fig. 2. A laser diode (LD, Teraxion PS-NLL) with a wavelength of 1550.12 nm and an output power of 18 dBm is served as the seed laser source, with a wavelength of 1550.12 nm. An optical power divider is used to divide the continuous-wave (CW) light into two equivalent parts. In the upper branch, the CW light is fed into a phase modulator (PM1, EOspace PM-DV5-40-PFA-PFA-LV) to generate the signal OFC. The 3-dB bandwidth and the half-wave voltage of PM1 are 40 GHz and 4.1 V, respectively. PM1 is driven by a single-tone signal of f_{S} generated from an RF source (RF1, Rohde&Schwarz SMA100B, 8 kHz–67 GHz). The dual-polarization CS-SSB modulator consists of two electrical hybrids (EH1 and EH2, Marki Microwave, QH0226 2–26.5 GHz) and a dual-polarization quadrature phase

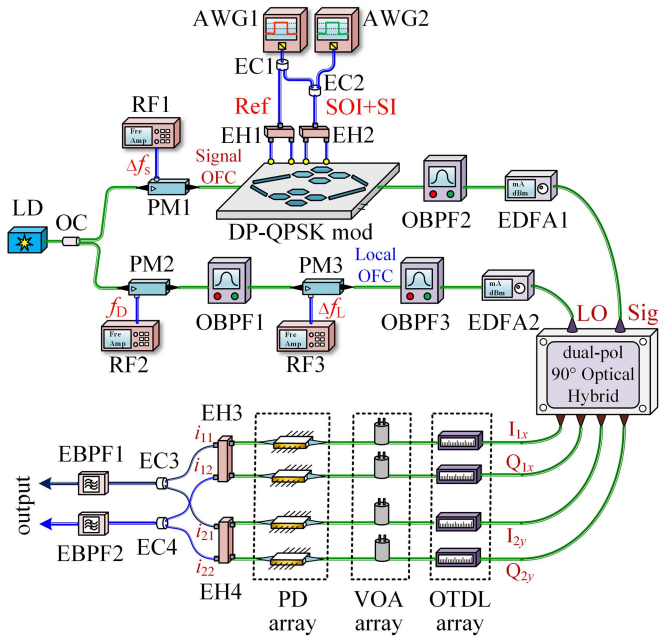

Fig. 2. Experimental setup of the proposed photonics-assisted approach for simultaneous RF channelization and self-interference cancellation. LD: laser diode; OC: optical coupler; AWG: arbitrary waveform generator; EC: electrical coupler; EH: electrical hybrid; DP-QPSK mod: dual-polarization quadrature phase shift keying modulator; MSG: microwave signal generator; PM: phase modulator; OBPF: optical bandpass filter; EDFA: erbium-doped fiber amplifier; VOA: variable optical attenuator; OTDL: optical tunable delay line; PD: photodetector; EBPF: electrical bandpass filter; Ref: reference signal; SOI: signal of interest; SI: self-interference signal.

shift keying (DP-QPSK) modulator (Fujitsu FTM7977 HQA). The DP-QPSK modulator has a working bandwidth of 23 GHz and a half-wave voltage of 3.5 V. Arbitrary waveform generator1 (AWG1, Keysight M8195A, 65 GSa/s) and AWG2 (Tektronix AWG70001A, 50 GSa/s) are used to generate the RF signals. The RF signal generated from AWG1 is divided into two parts. One part is used as the reference signal and injected into EH1. The other part is used as the self-interference signal, which is combined with the signal of interest generated from AWG2 and then injected to EH2. In the lower branch, the CW light is fed into PM2 (EOspace PM-DV5-40-PFA-PFA-LV) followed by an optical bandpass filter (OBPF1, Yenista XTM50) to realize the frequency shifting. An RF source (RF2, Rohde&Schwarz SMA100B, 8kHz–31.8 GHz) is used to generate a single-tone signal of f_{D} to drive PM2. After frequency shifting, PM3 (PM-5VEK-40-PFA-PFA-UV, 40 GHz) with a half-wave voltage of 3.2 V is inserted to generate the local OFC. In this way, the frequency difference of f_{D} between the center comb lines of the local OFC and signal OFC is realized. An RF source (RF3, Rohde&Schwarz SMA100B, 8kHz–40 GHz) is used to generate a single-tone signal of f_{L} to drive PM3. Two OBPFs (OBPF2 and OBPF3, Yenista XTM50) are used to realize the functions of multi-channel optical filters. Meanwhile, two erbium-doped fiber amplifiers (EDFAs, Amonics AEDFA-PA-35-B-FA) are incorporated in these two branches to compensate for the link loss. The dual-polarization 90-degree optical hybrid (Kylia COH28-00422) has a phase unbalance of 2° over the optical

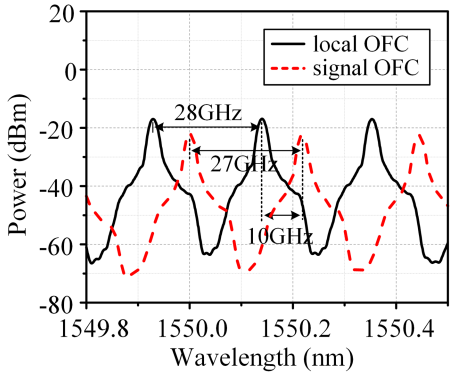

Fig. 3. Experimentally measured optical spectra of the generated signal OFC (in red dashed line) and local OFC (in black solid line).

wavelength range of 1520 to 1625 nm. The time delay module contains four parallel optical tunable delay lines (OTDLs, Sichuan Ziguan Photonics), which have a maximum delay range of 700ps and a delay resolution of 0.05ps. The attenuation module contains four parallel variable optical attenuators (VOAs, Sichuan Ziguan Photonics), which have a maximum attenuation range of 40 dB and an attenuation resolution of 0.05 dB. The 3-dB bandwidth and the responsivity of the photodetectors (PDs, CETC44 GD45216S) are 20 GHz and 0.8 A/W, respectively. The EBPFs (Talent Microwave TLBF-1G-3G-X) have a center frequency of 1.5 GHz, and the passing bandwidth is 1 GHz. A real-time oscilloscope (Tektronix DSA72004B, 50GSa/s) is used to observe the waveforms. An electrical spectrum analyzer (ESA, Rohde&Schwarz FSWP) and an optical spectrum analyzer (OSA, Yokogawa AQ6370C) are used to monitor the electrical spectra and the optical spectra, respectively.

B. The Performances of the Simultaneous Image-Rejection and Self-Interference Cancellation for the Microwave Photonic Image-Reject Mixers

The frequency intervals of the signal OFC and the local OFC (f_{S} and f_{L}) are set to be 27 and 28 GHz, respectively. The frequency shift f_{D} is set to 10 GHz. The optical spectra of the generated OFCs are plotted in Fig. 3. Both the signal OFC and the local OFC have three comb lines. The frequency differences of the 1st, 2nd and 3rd comb lines of the two OFCs are 9, 10, and 11 GHz, respectively.

Firstly, the isolation performances between the two channels corresponding to the same photonic LO are investigated. The wavelengths and the bandwidths of OBPF2 and OBPF3 are tuned properly to choose the 1st comb lines of the modulated signal OFC and the local OFC, respectively. EC3 is used to combine output port 1 of IRM$_x$ (i_{11}) and output port 1 of IRM$_y$ (i_{21}). EC4 is used to combine output port 2 of IRM$_x$ (i_{12}) and output port 2 of IRM$_y$ (i_{22}). LFM signals are used to verify the wide-bandwidth working performance. Two LFM signals of 7–8 and 10–11 GHz are applied on the CS-SSB modulator. The isolation performances between the two channels for the received RF signal are shown in Fig. 4(a-i) and (a-ii). Here the two LFM signals of 7–8 and 10–11 GHz are used as the received RF signal, while the reference signal is disconnected. The outputs from EC3 and EC4 are plotted as the blue and red solid lines, respectively. It can be noted that the frequency components of the optically-carried received RF signals located at 7–8 GHz and 10–11 GHz are both downconverted to the IF band of 1–2 GHz, and output from the two separated channels, respectively. The channel isolation ratio is larger than 28 dB over the whole 1–GHz bandwidth. The isolation performances between the two channels for the reference RF signal are shown in Fig. 4(b-i) and (b-ii). The two LFM signals of 7–8 and 10–11 GHz are used as the reference signal, while the received RF signal is disconnected. The outputs from EC3 and EC4 are plotted as the blue and red solid lines, respectively. The channel isolation ratio is about 29 dB over the whole 1–GHz bandwidth for the reference channel. In addition, these two pairs of downconverted components are phase-inversed. By connecting both the received RF signal and the reference signal, the outputs from EC3 and EC4 are given in Fig. 4(c). The phase inversion over the whole 1–GHz bandwidth is realized.

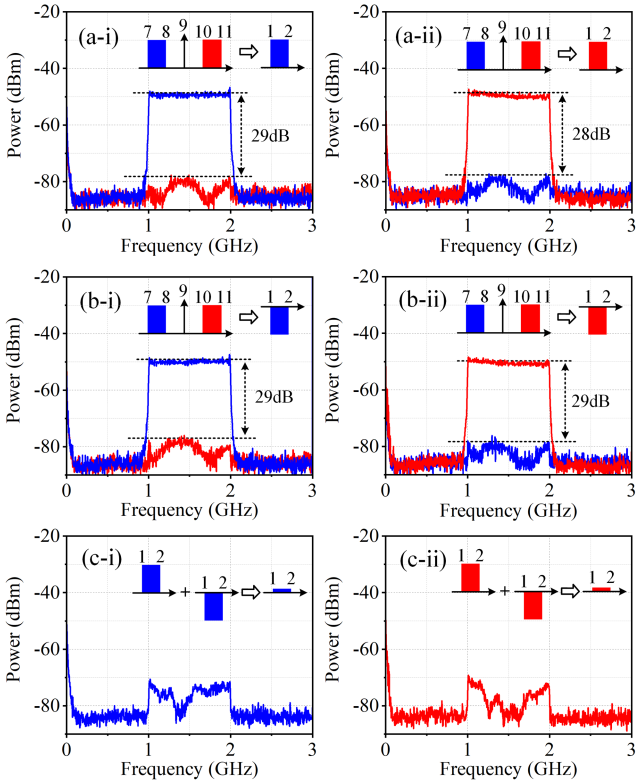

Fig. 4. Measured electrical spectra at the output of (i) EC3 and (ii) EC4 when (a) the received RF signal, and (b) reference signal, and (c) both the received RF signal and the reference signal are applied, respectively. Here, the 1st comb lines of the modulated signal OFC and local OFC are chosen.

Then, the performances of the simultaneous image-reject mixing and the self-interference cancellation are experimentally verified. An LFM signal of 7–8 GHz is used as the transmitted signal, and a single-tone at 7.5 GHz is served as the signal of interest. In this condition, the reference signal is an LFM signal of 7–8 GHz, while the received RF signal contains the self interference (an LFM signal of 7–8 GHz) and a signal of

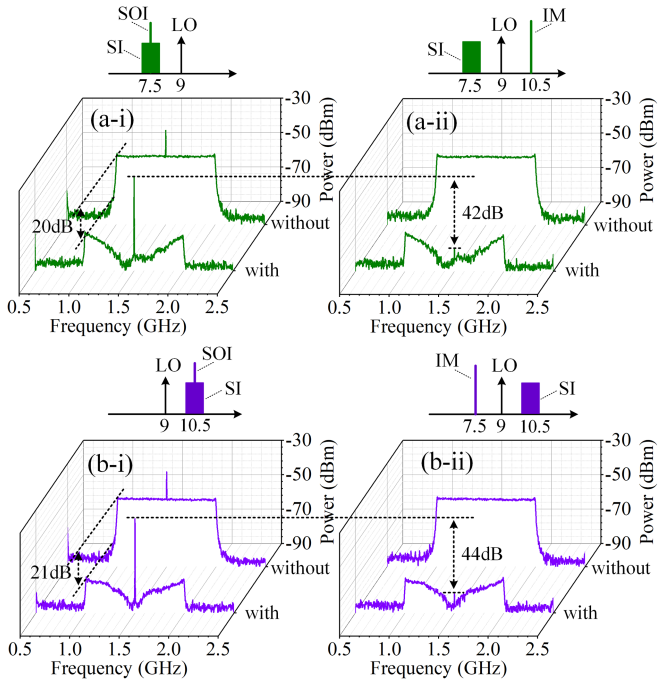

Fig. 5. Measured electrical spectra without and with self-interference cancellation at the output of (a) EC3 and (b) EC4 when (i) the signals of interest, and (ii) the image signals are applied. SOI: signal of interest; SI: self-interference; IM: image signal.

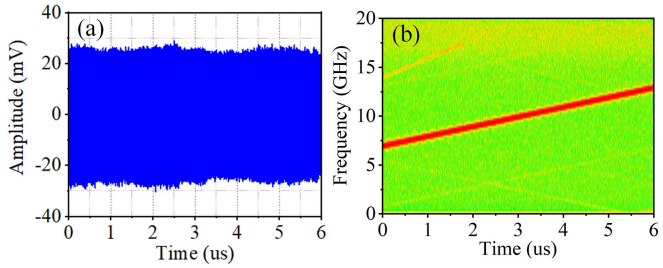

Fig. 6. Experimentally measured (a) waveform and (b) frequency-to-time curve of the transmitted signal (an LFM signal) to be channelized.

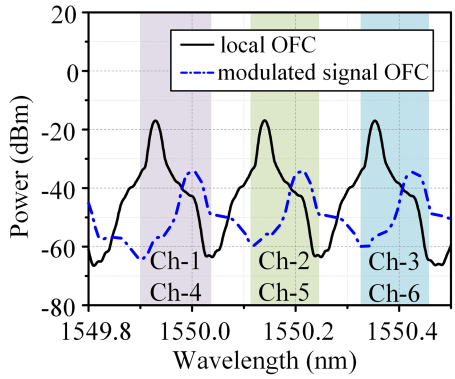

Fig. 7. Experimentally measured optical spectra of the modulated signal OFC (in blue dash-dotted line) and local OFC (in black solid line) when the transmitted signal of 7–13 GHz is applied.

interest (a single-tone signal at 7.5 GHz). The reference signal and the received RF signal are applied on the CS-SSB modulator. When the reference signal i_{21} is disconnected and connected, EC3 will output the downconverted results without and with the self-interference cancellation, being plotted in Fig. 5(a-i). As can be seen, the self-interference signal is well suppressed, with a cancellation depth of 20 dB. Meanwhile, the power of the signal of interest is kept unchanged. Then, an image signal at 10.5 GHz is used to replace the signal of interest at 7.5 GHz. The measured electrical spectra without and with the self-interference cancellation are shown in Fig. 5(a-ii). The downconverted image signal at 1.5 GHz is effectively suppressed, with an image-reject ratio of 42 dB. Meanwhile, the cancellation depth remains to be about 20 dB. The simultaneous image-reject mixing and self-interference cancellation are successfully realized.

Subsequently, the LFM signal is tuned to 10–11 GHz. Fig. 5(b-i) shows the downconverted results from EC4 without and with the self-interference cancellation when the signal of interest at 10.5 GHz is applied. Meanwhile, Fig. 5(b-ii) shows the output results without and with the self-interference cancellation when the image signal at 7.5 GHz is applied. The image-reject mixing with a 44-dB image-reject ratio, and the self-interference cancellation with a 21-dB cancellation depth are simultaneously achieved.

C. The Performances of the Simultaneous Channelization and Self-Interference Cancellation for the Proposed Microwave Photonic Channelizer

Then, the simultaneous channelization and self-interference cancellation performance of the proposed microwave photonic channelizer is investigated. Firstly, an LFM signal with a bandwidth of 6 GHz centered at 10 GHz is served as the received RF signal, which has a time duration of 6 μs. The measured waveform and the frequency-to-time diagram of the LFM signal are plotted in Fig. 6. The optical spectra of the modulated signal OFC and the local OFC are plotted in Fig. 7.

By tuning OBPF2 and OBPF3 to choose the corresponding comb lines of the modulated signal OFC and local OFC, two channels are output for each copy of the optically carried RF signal. Fig. 8(i) shows the electrical spectra of the channelized RF signal before and after bandpass filtering in each channel. The corresponding waveforms and frequency-to-time diagrams of the output signals in each channel are plotted in Fig. 8(ii). As shown in Fig. 8(a) and (b), the optically-carried RF components at the left and right sides of the 1st comb line of the local OFC are downconverted to the IF band simultaneously, shown as the black dashed lines. The bandwidths of these two IF signals are 2 and 4 GHz, respectively. After the electrical bandpass filtering, the channelized outputs centered at 1.5 GHz with a bandwidth of 1 GHz are generated from Ch-1 and Ch-4, plotted as the blue and red solid lines in Fig. 8(a-i) and (b-i), respectively. The unwanted spurs are suppressed to be about 20 dB within the whole 6-GHz bandwidth. The corresponding waveforms and frequency-to-time diagrams of the outputs from Ch-1 and Ch-4 are shown in Fig. 8(a-ii) and (b-ii), respectively.

Similarly, by selecting the 2nd comb line of the local OFC, the channelized outputs from Ch-2 and Ch-5 are obtained, as shown in Fig. 8(c) and (d), respectively. Fig. 8(e) and (f) show the channelized outputs from Ch-3 and Ch-6 with the 3rd comb

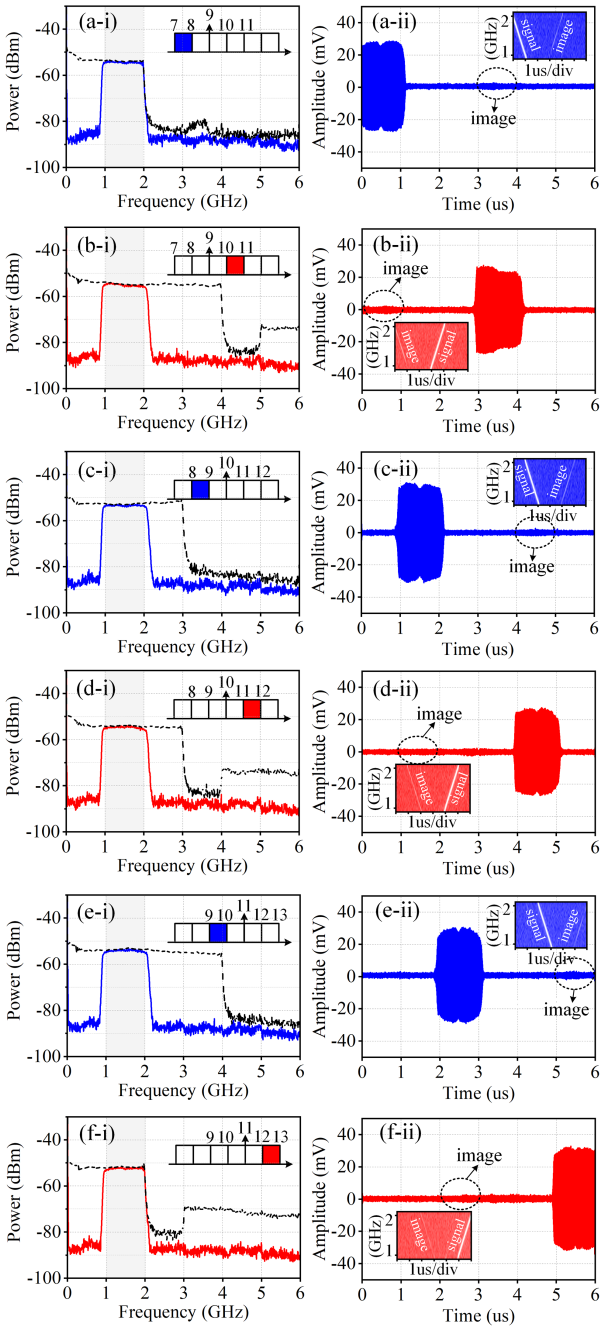

Fig. 8. Experimentally measured (i) electrical spectra of the channelized IF signals before (black dashed line) and after (blue/red solid line) the IF bandpass filtering, and (ii) the corresponding waveforms after IF bandpass filtering at the outputs of (a) Ch-1, (b) Ch-4, (c) Ch-2, (d) Ch-5, (e) Ch-3, and (f) Ch-6 when a signal of interest with a bandwidth of 6 GHz is applied. The insets in (ii) are the corresponding frequency-to-time diagrams.

line of the local OFC. The unwanted image components are well suppressed in all 6 channels. Therefore, the received RF signal with a 6-GHz bandwidth has been successfully channelized to 6 channels with a 1-GHz bandwidth.

Further experiments are also taken to investigate the simultaneous channelization and self-interference cancellation performances of the proposed system. An LFM signal with a bandwidth of 6 GHz centered at 10 GHz is served as the transmitted signal. For the observation of the cancellation performance in

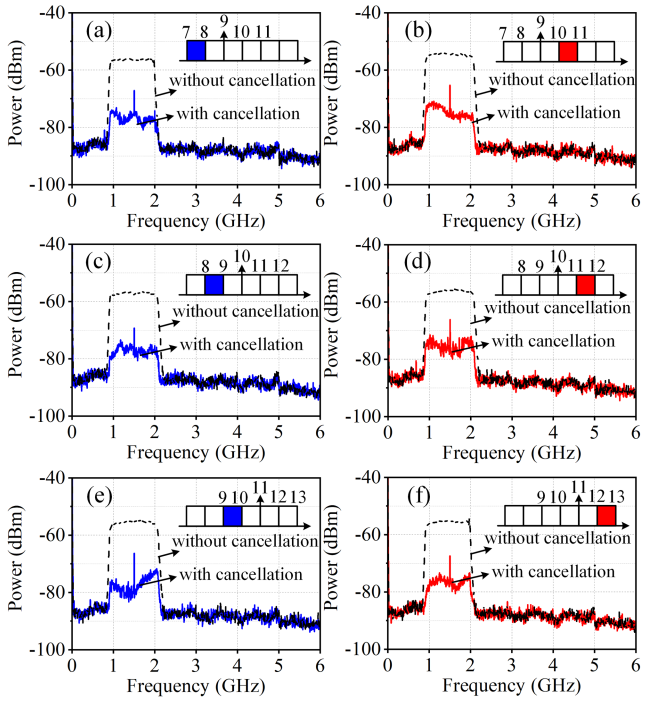

Fig. 9. Experimentally measured electrical spectra of the channelized output IF signals without (in black dashed lines) and with (in blue/red solid lines) self-interference cancellation of (a) Ch-1, (b) Ch-4, (c) Ch-2, (d) Ch-5, (e) Ch-3, and (f) Ch-6 when a transmitted signal with a bandwidth of 6 GHz is applied.

multi channels, a multi-tone signal with the frequency components of 7.5-, 8.5-, 9.5-, 10.5-, 11.5-, and 12.5-GHz is set to be the signal of interest. Fig. 9 shows the electrical spectra with and without the self-interference cancellation at the outputs of the six channels. As can be seen, the signal of interest of 7.5-, 8.5-, 9.5-, 10.5-, 11.5-, and 12.5-GHz are successfully channelized with the self-interference cancellated and output from each channel. The cancellation depths at Ch-1 to Ch-6 are 17-, 17-, 18-, 17-, 16-, and 18-dB, respectively. The simultaneous channelization and self-interference cancellation are successfully achieved over a 6-GHz bandwidth. The cancellation depth of larger than 16 dB is successfully obtained for all the channelized outputs.

Here the cancellation depth is smaller than that shown in Fig. 5. This is because in practical applications, the consistency of the phase, amplitude or time delay responses of the devices used in the system affect the cancellation depth. In Fig. 9, the performances are determined by the devices' response consistency over the 6-GHz bandwidth. While in Fig. 5, the performance is determined by the devices' response consistency over the 1-GHz bandwidth. By improving the devices' consistency, i.e., through implementing the on-chip integration, the cancellation depth over a large bandwidth can be improved.

IV. Conclusion

In conclusion, a photonics-assisted RF receiver for simultaneous RF channelization and self-interference cancellation has been proposed and demonstrated. Dual optical frequency combs and microwave photonic IRMs using a dual-output Hartley structure are used. Combing the polarization multiplexing technique, two channels of the signal of interest are obtained with each local

OFC comb line, while both the image signal component and the self-interference component in each channel are eliminated simultaneously. The matching of the phase, time delay, and amplitude among the microwave photonic channelization paths, and between the reference signal and the self-interference signal are all implemented by photonic methods, guaranteeing the simultaneous channelization and self-interference cancellation over a wide bandwidth. The simultaneous channelization and self-interference cancellation are experimentally realized over a 6-GHz bandwidth, and 6 output channels are obtained. The performance of the proposed approach is demonstrated by discrete devices in our experiment. The integration is an improvement direction with the system [28], [29]. By introducing on-chip integrating techniques, the system integration and miniaturization will be achieved. The system' response over a wide bandwidth will become better, improving the performance. The proposed approach can find applications in future cognitive RF systems such as radar, electronic warfare, and wireless communication to enable the in-band full-duplex operations.

REFERENCES

[1] S. Hong et al., "Applications of self-interference cancellation in 5G and beyond," *IEEE Commun. Mag.*, vol. 52, no. 2, pp. 114–121, Feb. 2014.

[2] T. Riihonen, D. Korpi, O. Rantula, H. Rantanen, T. Saarelainen, and M. Valkama, "Inband full-duplex radio transceivers: A paradigm shift in tactical communications and electronic warfare?," *IEEE Commun. Mag.*, vol. 55, no. 10, pp. 30–36, Oct. 2017.

[3] I. Brodsky, J. Brand, and M. Jain, "Freedom of frequency: How the quest for in-band full-duplex led to a breakthrough in filter design," *IEEE Microw. Mag.*, vol. 20, no. 2, pp. 36–43, Feb. 2019.

[4] D. Zhu and S. Pan, "Broadband cognitive radio enabled by photonics," *J. Lightw. Technol.*, vol. 38, no. 12, pp. 3076–3088, Jun. 2020.

[5] W. Namgoong, "A channelized digital ultrawideband receiver," *IEEE Trans. Wireless Commun.*, vol. 2, no. 3, pp. 502–510, May 2003.

[6] S. T. Winnall, A. C. Lindsay, M.W. Austin, J. Canning, and A. Mitchell, "A microwave channelizer and spectroscope based on an integrated optical Bragg-grating Fabry-Perot and integrated hybrid Fresnel lens system," *IEEE Trans. Microw. Theory Techn.*, vol. 54, no. 2, pp. 868–872, Feb. 2006.

[7] X. Zou, W. Pan, B. Luo, and L. Yan, "Photonic approach for multiple-frequency-component measurement using spectrally sliced incoherent source," *Opt. Lett.*, vol. 35, no. 3, pp. 438–440, Feb. 2010.

[8] X. Xie et al., "Broadband photonic radio-frequency channelization based on a 39-GHz optical frequency comb," *IEEE Photon. Technol. Lett.*, vol. 24, no. 8, pp. 661–663, Apr. 2012.

[9] H. Huang, C. Zhang, H. Zhou, H. Yang, W. Yuan, and K. Qiu, "Double-efficiency photonic channelization enabling optical carrier power suppression," *Opt. Lett.*, vol. 43, no. 17, pp. 4073–4076, Sep. 2018.

[10] Z. Tang, D. Zhu, and S. Pan, "Coherent optical RF channelizer with large instantaneous bandwidth and large in-band interference suppression," *J. Lightw. Technol.*, vol. 36, no. 19, pp. 4219–4226, Oct. 2018.

[11] D. Zhu, W. Chen, and C. Xie, "Microwave channelizer based on a photonic dual-output image-reject mixer," *Opt. Lett.*, vol. 44, no. 16, pp. 4052–4055, Aug. 2019.

[12] H. Huang, R. Wang, C. Zhang, Y. Chen, H. Yang, and K. Qiu, "Tunable ultra-flat optical-comb-enabled, reconfigurable, and efficient coherent channelized receiver," *Opt. Lett.*, vol. 45, no. 4, pp. 848–851, Feb. 2020.

[13] W. Zhai, A. Wen, Y. Gao, D. Shan, and Y. Fan, "An ultraefficient broadband photonic channelizer based on polarization-division multiplexing and integrated dual-polarization coherent detection receiver," *IEEE Trans. Microw. Theory Techn.*, vol. 70, no. 3, pp. 1821–1831, Mar. 2022.

[14] X. Han et al., "RF self-interference cancellation by using photonic technology," *Chin. Opt. Lett.*, vol. 19, no. 7, Jul. 2021, Art. no. 073901.

[15] J. Suarez, K. Kravtsov, and P. R. Prucnal, "Incoherent method of optical interference cancellation for radio-frequency communications," *IEEE J. Quantum Electron.*, vol. 45, no. 4, pp. 402–408, Apr. 2009.

[16] Y. Chen and S. Pan, "Simultaneous wideband radio-frequency self-interference cancellation and frequency downconversion for in-band full-duplex radio-over-fiber systems," *Opt. Lett.*, vol. 43, no. 13, pp. 3124–3127, Jul. 2018.

[17] Y. Chen, "A photonic-based wideband RF self-interference cancellation approach with fiber dispersion immunity," *J. Lightw. Technol.*, vol. 38, no. 17, pp. 4618–4624, Sep. 2020.

[18] H. Song et al., "Simultaneous RF self-interference cancellation, local oscillator generation, frequency up- and down-conversion in an integrated in-band full-duplex 5G RF transceiver front-end," *J. Lightw. Technol.*, vol. 40, no. 2, pp. 511–518, Jan. 2022.

[19] P. Li et al., "Photonic-assisted leakage cancellation for wideband frequency modulation continuous-wave radar transceiver," *J. Lightw. Technol.*, vol. 38, no. 6, pp. 1178–1183, Mar. 2020.

[20] J. Wang, H. Yu, Z. Zhao, Z. Zhang, and J. Liu, "Photo-assisted self-interference cancellation for in-band full-duplex radio-over-fiber system," *Appl. Opt.*, vol. 60, no. 11, pp. 3021–3030, Apr. 2021.

[21] Z. Zhu et al., "Photonics-assisted ultrawideband RF self-interference cancellation with signal of interest recovery and fiber transmission," *J. Lightw. Technol.*, vol. 40, no. 3, pp. 655–663, Feb. 2022.

[22] M. P. Chang, M. Fok, A. Hofmaier, and P. R. Prucnal, "Optical analog self-interference cancellation using electro-absorption modulators," *IEEE Microw. Wireless Compon. Lett.*, vol. 23, no. 2, pp. 99–101, Feb. 2013.

[23] Y. Xiang, G. Li, and S. Pan, "Ultrawideband optical cancellation of RF interference with phase change," *Opt. Exp.*, vol. 25, no. 18, pp. 21259–21264, Sep. 2017.

[24] D. Zhu, X. Hu, W. Chen, D. Ben, and S. Pan, "Photonics-enabled simultaneous self-interference cancellation and image-reject mixing," *Opt. Lett.*, vol. 44, no. 22, pp. 5541–5544, Nov. 2019.

[25] X. Hu, D. Zhu, L. Li, and S. Pan, "Photonics-based adaptive RF self-interference cancellation and frequency downconversion," *J. Lightw. Technol.*, vol. 40, no. 7, pp. 1989–1999, Apr. 2022.

[26] F. Shi et al., "A microwave photonic channelized receiver with self-interference cancellation," *J. Lightw. Technol.*, vol. 41, no. 2, pp. 627–636, Jan. 2023.

[27] Kylia, "90 degree hybrids or coherent receivers." Feb. 24, 2015. [Online] Available: https://kylia.com/90-hybrids

[28] H. Jiang, L. Yan, and D. Marpaung, "Chip-based arbitrary radio-frequency photonic filter with algorithm-driven reconfigurable resolution," *Opt. Lett.*, vol. 43, no. 3, pp. 415–418, Feb. 2018.

[29] Y. Liu et al., "Tuning optimization of ring resonator delays for integrated optical beam forming networks," *J. Lightw. Technol.*, vol. 35, no. 22, pp. 4954–4960, Nov. 2017.

Xiaopeng Hu received the B.S. degree in communication engineering from the Nanjing University of Posts and Telecommunications, Nanjing, China, in 2015, and the M.S. degree in signal processing from the Jiangsu University of Science and Technology, Zhenjiang, China, in 2018. He is currently working toward the Ph.D. degree with Nanjing University of Aeronautics and Astronautics, Nanjing. His research interests include photonic signal processing and photonics-based RF front-end.

Dan Zhu (Member, IEEE) received the B.S. and Ph.D. degrees in electronic engineering from Tsinghua University, Beijing, China, in 2004 and 2009, respectively. In May 2011, she joined the College of Electronic and Information Engineering, Nanjing University of Aeronautics and Astronautics, Nanjing, China, where she is currently a Professor. From May 2014 to May 2015, she was a Visiting Scholar with the Microwave Photonics Research Laboratory, University of Ottawa, Ottawa, ON, Canada. Her research interests include microwave photonic signal processing and the system applications. She is a Member of the IEEE Microwave Theory and Techniques Society, IEEE Photonics Society, and Optical Society of America.

Shuo Liu received the B.S. degree in electronic information engineering from the China University of Mining and Technology, Xuzhou, China, in 2020. She is currently working toward the M.S. degree with the Nanjing University of Aeronautics and Astronautics, Nanjing, China. Her research focuses on microwave photonic processing.

Hai Xiao received the B.S. degree in electronic information engineering from Dalian Maritime University, Dalian, China, in 2020. He is currently working toward the M.S. degree with the Nanjing University of Aeronautics and Astronautics, Nanjing, China. His research focuses on microwave photonic processing.

Shilong Pan (Fellow, IEEE) received the B.S. and Ph.D. degrees in electronic engineering from Tsinghua University, Beijing, China, in 2004 and 2008, respectively. From 2008 to 2010, he was a "Vision 2010" Postdoctoral Research Fellow with the Microwave Photonics Research Laboratory, University of Ottawa, Ottawa, ON, Canada. In 2010, he joined the College of Electronic and Information Engineering, Nanjing University of Aeronautics and Astronautics, Nanjing, China, where he is currently a Full Professor and the Director of the National Key Laboratory of Microwave Photonics.

His research focuses on microwave photonics, which includes optical generation and processing of microwave signals, analog photonic links, photonic microwave measurement, and integrated microwave photonics.

He is currently the Deputy Editor of *Chinese Optics Letters*, an Associate Editor of the *Journal of Lightwave Technology*, IEEE TRANSACTIONS ON MICROWAVE THEORY AND TECHNIQUES, and *Electronics Letters*, and is the Vice Chair of IEEE MTT-22 Microwave Photonics. He was the Chair of a number of international conferences, symposia, and workshops, including the TPC Chair of the ICOCN 2015, TPC Chair of IEEE MWP in 2023, TPC Co-Chair of IEEE MWP 2017, and General Co-chair of IEEE MWP 2021.

He is a Fellow of IEEE, Optica, SPIE, and IET. He was selected as an IEEE Photonics Society Distinguished Lecturer in 2019 and an IEEE MTT-S Distinguished Microwave Lecturer in 2022. He was the recipient of the IEEE MTT-S Outstanding Young Engineer Award in 2021.